Spatial patterns of neuroimaging biomarker change in individuals from families with autosomal dominant Alzheimer's disease: a longitudinal study

Brian A Gordon, Tyler M Blazey*, Yi Su, Amrita Hari-Raj, Aylin Dincer, Shaney Flores, Jon Christensen, Eric McDade, Guoqiao Wang, Chengjie Xiong, Nigel J Cairns, Jason Hassenstab, Daniel S Marcus, Anne M Fagan, Clifford R Jack Jr, Russ C Hornbeck, Katrina L Paumier, Beau M Ances, Sarah B Berman, Adam M Brickman, David M Cash, Jasmeer P Chhatwal, Stephen Correia, Stefan Förster, Nick C Fox, Neill R Graff-Radford, Christian la Fougère, Johannes Levin, Colin L Masters, Martin N Rossor, Stephen Salloway, Andrew J Saykin, Peter R Schofield, Paul M Thompson, Michael M Weiner, David M Holtzman, Marcus E Raichle, John C Morris, Randall J Bateman, Tammie L S Benzinger*

Summary

Background Models of Alzheimer's disease propose a sequence of amyloid β (Aβ) accumulation, hypometabolism, and structural decline that precedes the onset of clinical dementia. These pathological features evolve both temporally and spatially in the brain. In this study, we aimed to characterise where in the brain and when in the course of the disease neuroimaging biomarkers become abnormal.

Methods Between Jan 1, 2009, and Dec 31, 2015, we analysed data from mutation non-carriers, asymptomatic carriers, and symptomatic carriers from families carrying gene mutations in presenilin 1 (*PSEN1*), presenilin 2 (*PSEN2*), or amyloid precursor protein (*APP*) enrolled in the Dominantly Inherited Alzheimer's Network. We analysed ^{11}C-Pittsburgh Compound B (^{11}C-PiB) PET, ^{18}F-Fluorodeoxyglucose (^{18}F-FDG) PET, and structural MRI data using regions of interest to assess change throughout the brain. We estimated rates of biomarker change as a function of estimated years to symptom onset at baseline using linear mixed-effects models and determined the earliest point at which biomarker trajectories differed between mutation carriers and non-carriers. This study is registered at ClinicalTrials.gov (number NCT00869817).

Findings ^{11}C-PiB PET was available for 346 individuals (162 with longitudinal imaging), ^{18}F-FDG PET was available for 352 individuals (175 with longitudinal imaging), and MRI data were available for 377 individuals (201 with longitudinal imaging). We found a sequence to pathological changes, with rates of Aβ deposition in mutation carriers being significantly different from those in non-carriers first (across regions that showed a significant difference, at a mean of 18·9 years [SD 3·3] before expected onset), followed by hypometabolism (14·1 years [5·1] before expected onset), and lastly structural decline (4·7 years [4·2] before expected onset). This biomarker ordering was preserved in most, but not all, regions. The temporal emergence within a biomarker varied across the brain, with the precuneus being the first cortical region for each method to show divergence between groups (22·2 years before expected onset for Aβ accumulation, 18·8 years before expected onset for hypometabolism, and 13·0 years before expected onset for cortical thinning).

Interpretation Mutation carriers had elevations in Aβ deposition, reduced glucose metabolism, and cortical thinning compared with non-carriers which preceded the expected onset of dementia. Accrual of these pathologies varied throughout the brain, suggesting differential regional and temporal vulnerabilities to Aβ, metabolic decline, and structural atrophy, which should be taken into account when using biomarkers in a clinical setting as well as designing and evaluating clinical trials.

Funding US National Institutes of Health, the German Center for Neurodegenerative Diseases, and the Medical Research Council Dementias Platform UK.

Introduction

Alzheimer's disease presents as a progressive loss of cognitive function, leading to severe impairment and loss of independence. Alzheimer's disease's long preclinical phase has bolstered efforts to identify in-vivo biomarkers to aid disease diagnosis and prognosis.[1] Models of Alzheimer's disease pathophysiology theorise a temporal sequence in which disruptions in amyloid β (Aβ) production, clearance, or both initiates a biological cascade that leads to Aβ plaque formation that spreads throughout the cortex, followed by tauopathy, neuronal dysfunction, neuronal death, and ultimately dementia.[2,3]

PET and MRI can be used to assess both the amount and location of Aβ plaques, tauopathy (eg, tau-containing neurofibrillary tangles and neuropil), altered glucose metabolism, and structural decline. The temporal sequence of these biomarkers provides information about the pathogenesis of Alzheimer's disease. Determining the order of changes in sporadic

Lancet Neurol 2018; 17: 241–50

Published Online January 31, 2018 http://dx.doi.org/10.1016/S1474-4422(18)30028-0

See Comment page 199

*Contributed equally

Mallinckrodt Institute of Radiology (B A Gordon PhD, T M Blazey BS, Y Su PhD, A Hari-Raj BA, A Dincer BA, S Flores BS, J Christensen BS, D S Marcus PhD, R C Hornbeck MS, Prof M E Raichle MD, T L S Benzinger MD), **Knight Alzheimer's Disease Research Center** (B A Gordon, Prof C Xiong PhD, Prof N J Cairns PhD, J Hassenstab PhD, Prof A M Fagan PhD, Prof D M Holtzman MD, Prof J C Morris MD, Prof R J Bateman MD, T L S Benzinger), **Division of Biology and Biomedical Sciences** (T M Blazey), **Department of Neurology** (E McDade DO, G Wang PhD, Prof N J Cairns, J Hassenstab, Prof A M Fagan, K L Paumier PhD, Prof B M Ances MD, Prof D M Holtzman, Prof M E Raichle, Prof J C Morris, Prof R J Bateman), **Department of Biostatistics** (Prof C Xiong), **and Department of Psychological & Brain Sciences** (J Hassenstab, B A Gordon), **Washington University, St Louis, MO, USA; The Hope Center for Neurological Disorders, St Louis, MO, USA** (Prof A M Fagan, Prof B M Ances, Prof D M Holtzman, Prof M E Raichle, Prof R J Bateman); **Department of Radiology, Mayo Clinic and Foundation, Rochester, MN, USA** (Prof C R Jack Jr MD); **Department of Neurology, University of Pittsburgh,**

Pittsburgh, PA, USA (S B Berman MD); **Taub Institute for Research on Alzheimer's Disease and the Aging Brain, College of Physicians and Surgeons** (A M Brickman PhD), **and Department of Neurology** (A M Brickman), **Columbia University, New York, NY, USA; Dementia Research Centre, Department of Neurodegenerative Disease, Institute of Neurology** (D M Cash PhD, Prof N C Fox MD, Prof M N Rossor MD), **and Translational Imaging Group, Centre for Medical Image Computing** (D M Cash), **University College London, London, UK; Department of Neurology, Massachusetts General Hospital, Harvard Medical School, Boston, MA, USA** (J P Chhatwal MD); **Department of Psychiatry** (S Correia PhD, Prof S Salloway MD) **and Department of Neurology** (Prof S Salloway), **Brown University School of Medicine, Providence, RI, USA; Department of Nuclear Medicine, Technische Universität München, Munich, Germany** (S Förster MD); **German Center for Neurodegenerative Diseases (DZNE) Munich, Munich, Germany** (S Förster, J Levin MD); **German Center for Neurodegenerative Diseases (DZNE) Tübingen, Tübingen, Germany** (S Förster, Prof C la Fougère MD); **Department of Neurology, Mayo Clinic, Jacksonville, FL, USA** (Prof N R Graff-Radford MD); **Division of Nuclear Medicine and Clinical Molecular Imaging, University Hospital Tübingen, Tübingen, Germany** (Prof C la Fougère); **Department of Neurology, Ludwig-Maximilians-Universität München, Munich, Germany** (J Levin); **The Florey Institute, University of Melbourne, Parkville, VIC, Australia** (Prof C L Masters MD); **Brown University School of Medicine, Providence, RI, USA; Indiana University School of Medicine, Indianapolis, IN, USA** (Prof A J Saykin PsyD); **Neuroscience Research Australia, Sydney, NSW, Australia** (Prof P R Schofield DSc); **School of Medical Sciences, University of New South Wales, Sydney**

Research in context

Evidence before this study

We reviewed previous work on longitudinal neuroimaging markers of Alzheimer's disease pathology with a focus on autosomal dominant Alzheimer's disease. We searched PubMed and Google Scholar for all articles published from database inception to Oct 31, 2017, with no language restrictions, for the keywords "Alzheimer's", "Alzheimer", "longitudinal", "positron emission tomography", "PET", "MRI", "atrophy", "FDG", "hypometabolism", "familial", and "autosomal". Theories proposed initially in 2010 by Jack and colleagues and revised in 2013 posited temporal trajectories of Alzheimer's disease biomarkers relative to each other and clinical decline. Work by Bateman and colleagues in 2012, Benzinger and colleagues in 2013, and Fleisher and colleagues in 2015 depict such temporal ordering of biomarkers in autosomal dominant Alzheimer's disease populations derived from cross-sectional analyses. There was also a small subset of longitudinal studies, but these had one or more limitations such as small populations (n<50), examination of only one biomarker, not accounting for regional differences or correlations in the brain, or a short duration of longitudinal follow up.

Added value of this study

To our knowledge, our study presents the first known work examining both the longitudinal temporal trajectories and the spatial patterns of Alzheimer's disease pathology in autosomal dominant Alzheimer's disease cohorts using neuroimaging. This work also presents the largest known cohort to date of individuals with autosomal dominant Alzheimer's disease studied longitudinally with multiple neuroimaging biomarkers. Longitudinal analyses can provide a more accurate and powerful way to model the temporal emergence of pathology in autosomal dominant Alzheimer's disease. We find that mutation carriers first display amyloid β accumulation, followed by hypometabolism, and finally structural atrophy; this is consistent with theoretical models and cross-sectional estimates from autosomal dominant Alzheimer's disease. Most importantly we consider such temporal relationships not in one singular summary measure, but characterise these trajectories throughout the brain. We found that the accrual of pathology varied throughout the brain and by method in terms of the time of initial emergence and the rates of longitudinal change. These findings suggest region-specific vulnerabilities to β-amyloidosis, metabolic decline, and atrophy that change over the course of the disease.

Implications of all the available evidence

Our results build upon existing evidence characterising biomarkers in clinical and preclinical Alzheimer's disease. Our findings suggest that imaging biomarkers follow a sequential pattern, with β-amyloidosis, hypometabolism, and structural atrophy emerging more than 20, 15, and 10 years, respectively, before the expected onset of dementia. Although there is a general hierarchical pattern, there was considerable regional heterogeneity. The most common deviation from the pattern of β-amyloidosis, followed by hypometabolism, followed by structural atrophy was that regions showed an increase in β-amyloidosis and structural atrophy but no evidence of metabolic decline. Furthermore, rather than being homogeneous, the same biomarker often shows different longitudinal trajectories across brain regions. Characterising the temporal and regional dynamics of biomarkers in Alzheimer's disease provides insight into disease pathophysiology. This information is crucial to decide how to best use neuroimaging biomarkers in clinical trials for participant selection as well as for outcomes measures.

Alzheimer's disease is problematic because it is difficult to predict an individual's relative position in the disease. Autosomal dominant Alzheimer's disease is well suited to study biomarker trajectories owing to the virtually complete penetrance of the mutations and consistency of symptom onset within families.[4,5] The conserved onset age within families and mutation types allows individuals to be staged relative to their expected onset of symptoms.

Research on autosomal dominant Alzheimer's disease has revealed a temporal ordering of biomarkers consistent with theoretical models,[6–8] and indicates that pathology progressively appears in new regions of the brain as the disease worsens.[7] These findings have primarily relied on cross-sectional analyses, with few longitudinal studies done, and mainly using small cohorts.[7,9–16] Longitudinal analyses can provide a better estimate of the true pathological trajectories.[17,18] This is crucial because interventional trials such as the Dominantly Inherited Alzheimer Network (DIAN) Trials Unit,[19] the Alzheimer's Prevention Initiative (API),[20] and the Anti-Amyloid Treatment in Asymptomatic Alzheimer's Study (A4)[21] will all evaluate alterations in longitudinal biomarker trajectories.

The DIAN observational study[4] has established a large cohort of families with autosomal dominant Alzheimer's disease and longitudinal Aβ, metabolic, and structural neuroimaging assessments of family members. Our current work compares rates of biomarker change in a large population of mutation carriers and non-carriers throughout the entire brain. In this way we can visualise when pathology biomarkers first emerge and how they spread throughout the course of the disease.

Methods

Study design and participants

Individuals from families known to have mutations in the presenilin 1 (*PSEN1*), presenilin 2 (*PSEN2*), and amyloid precursor protein (*APP*) genes were recruited from 14 sites participating in the DIAN observational study in the USA, UK, Germany, and Australia. All participants with genetic, clinical, and neuroimaging

data that passed quality control from the 10th semiannual data freeze were included in the analyses. The institutional review board at Washington University (St Louis, MO, USA) provided supervisory review and human studies approval. Participants or their caregivers provided written informed consent in accordance with their local institutional review board. Clinical and imaging visits in DIAN are performed every 3 years for asymptomatic individuals until they are within 3 years of their parental age of dementia onset. Assessments become annual once an individual is within 3 years of parental age at onset or if an individual becomes symptomatic. Analyses excluded families with the Dutch and Flemish mutations in *APP*, because these mutations often present with predominant cerebral amyloid angiopathy and diffuse Aβ plaques (appendix).

Procedures

Dementia status was assessed using the Clinical Dementia Rating.[22] For each visit, a participant's estimated years from expected symptom onset was calculated on the basis of the participant's current age relative to either the family mutation-specific expected age at dementia onset[5] or parental age at first progressive cognitive decline if expected age at onset for the mutation was unknown. A mutation-specific expected age of dementia onset is calculated by integrating the age of onset reported in the literature across individuals with the same specific mutation.[5] Expected symptom onset was established identically for both carriers and non-carriers. The presence or absence of an autosomal dominant Alzheimer's disease mutation was determined using PCR-based amplification of the appropriate exon followed by Sanger sequencing.[6] Clinical evaluators were masked to mutation status of participants.

MRI was done using the Alzheimer's Disease Neuroimaging Initiative (ADNI) protocol.[23] Sites used a 3T scanner and were required to pass regular quality control assessments. T1-weighted images (1·1×1·1×1·2 mm voxels) were acquired for all participants. The ADNI Imaging Core screened images for protocol compliance and artifacts. Volumetric segmentation and cortical surface reconstruction was done using FreeSurfer 5.3,[24,25] which automatically defines subcortical and cortical regions of interest (ROIs). Segmentations were inspected by members of the DIAN Imaging Core and edited as needed. Subcortical volumes were corrected for intracranial volume using a regression approach. Cortical thickness and volume measures were averaged across hemispheres. The cortical and subcortical labels identified on the MRI were used for the regional processing of all PET data. For all analyses, we examined 34 cortical ROIs and seven subcortical ROIs. A full list of regions is available in the appendix.

Aβ imaging was done using a bolus injection of ^{11}C-Pittsburgh Compound B (^{11}C-PiB). Acquisition consisted of a 70-min scan starting at injection or a 30-min scan beginning 40 min after injection. Data in the common 40–70 min timeframe was converted to regional standardised uptake value ratios (SUVRs) relative to the cerebellar grey matter using FreeSurfer-derived ROIs[26] (PET Unified Pipeline). Metabolic imaging was done with ^{18}F-Fluorodeoxyglucose (^{18}F-FDG) with a 30 min dynamic acquisition beginning 30 min after injection. Data from the last 20 min of each ^{18}F-FDG scan were converted to SUVRs relative to cerebellar grey matter. Both types of PET data were partial volume corrected using a regional spread function technique.[27,28]

Because we did not have a priori laterality predictions, data were averaged across hemispheres before being entered into statistical analyses. Differences in spatial resolution across PET scanners were accounted for by applying scanner-specific spatial filters to achieve a common resolution (8 mm).[29] The ADNI PET Core verified that PET images were acquired using the established protocol and free of substantial artifacts.

Statistical analysis

We used multivariate linear mixed-effects models to describe the evolution of Alzheimer's disease biomarkers. Linear mixed-effects models have many benefits, including providing a flexible approach to deal with an unequal number of measurement points or intervals. Although neuroimaging analyses traditionally use univariate models, the field has begun using multivariate models that account for correlations between regional or voxelwise measurements.[30–32] Multivariate linear mixed-effects models can increase statistical power and reliability compared with univariate methods.[30,31] We implemented a Bayesian multivariate linear mixed-effects model to compare longitudinal biomarker changes directly across brain regions. Cortical and subcortical measurements were analysed separately for each method (^{11}C-PiB, ^{18}F-FDG, and MRI), resulting in a total of six independent models.

The full Bayesian linear mixed-effects model is described in the appendix. Each region included fixed effects for mutation status, time from baseline, baseline estimated years from symptom onset, and all possible two-way and three-way interactions. Estimated years from expected symptom onset was modelled as a restricted cubic spline with knots at the 0·10, 0·50, and 0·90 quantiles. We chose restricted cubic splines to model estimated years from expected symptom onset because they represent a flexible approach for accounting for non-linearities in the data without forcing any particular curve shape. Splines have also been used extensively in the literature to model longitudinal changes in Alzheimer's disease biomarkers.[33,34] For every region we included random intercepts and slopes at the participant-level, as well as random intercepts for family affiliation. At the participant-level, covariance matrices were constructed

NSW, Australia (Prof P R Schofield); **Imaging Genetics Center, University of Southern California, Marina del Rey, CA, USA** (Prof P M Thompson PhD); **and Department of Radiology and Biomedical Imaging, University of California, San Francisco, CA, USA** (Prof M M Weiner MD)

Correspondence to:
Dr Brian A Gordon, Mallinckrodt Institute of Radiology, Washington University, St Louis, MO 63110, USA
bagordon@wustl.edu

For more on the **DIAN observational study** see http://www.dian-info.org

For the **PET Unified Pipeline** see https://github.com/ysu001/PUP

See **Online** for appendix

so that intercepts and the slopes were allowed to correlate across all regions in a model.

For **Stan** see http://mc-stan.org/

To fit each model we used Stan,[35,36] an open source package for Hamilton Markov chain Monte Carlo analyses. A parameter, or combination of parameters, was considered statistically significant if the 99% equal-tailed credible intervals of the posterior distribution did not overlap zero. Analyses were run separately for each method (MRI, ^{11}C-PiB, and ^{18}F-FDG). Within each method, one model simultaneously fit 34 cortical ROIs and a second model simultaneously fit seven subcortical ROIs derived from FreeSurfer. Each regional comparison within a model is simply a different slice of the same multidimensional posterior distribution. The current analyses focus on the interaction between mutation status and the longitudinal rate of change. Including multiple regions within one model also allows for the direct comparison of rates of changes between regions (appendix). Data from the DIAN project can be requested freely by researchers.

For data from the **DIAN project** see https://dian.wustl.edu/our-research/observational-study/dian-observational-study-investigator-resources/

Role of the funding source

The study sponsors had no role in the study design, data collection, data analysis, data interpretation, writing of the report, or the decision to submit the manuscript for publication. All authors had full access to the data in the study and the corresponding author had final responsibility for the decision to submit for publication.

Results

Participants were recruited between Jan 1, 2009, and Dec 31, 2015 (table 1). The analyses included 346 individuals with ^{11}C-PIB PET Aβ data, 352 with ^{18}F-FDG PET metabolism data, and 377 with MRI volumetric data (table 2). Participants with longitudinal data had a mean of 2·4 visits (SD 0·8) and 2·7 years (SD 1·1) of data. Figure 1 shows example linear mixed-effects model fits for one region, the precuneus, which was the first region to show a difference between mutation carriers and non-carriers for each imaging method. Figures depicting the model results for every ROI are accessible via a link in the appendix. To avoid inadvertently revealing participants' mutation status at the edges of our sample for which there are only a few individuals, figures are displayed with baseline estimated years to symptom onset of –29 years to +10 years.

The rate of Aβ accumulation was significantly higher in mutation carriers relative to non-carriers starting more than two decades before the expected age of dementia onset (–22·2 years; figure 1). Because glucose use represents a natural biological property it contains both maturational and disease-related trajectories. In both groups, the precuneus ^{18}F-FDG trajectories were initially positive, slowed and showed little annual change, and then became negative. This negative directional acceleration began earlier and was larger in participants with mutations, with the rate of change in metabolism diverging from those without mutations an estimated 18·8 years before expected symptom onset. Finally, precuneus cortical thinning significantly differed in mutation carriers relative to those without mutations at 13·0 years before estimated expected symptom onset. The appendix contains a link to an application for viewing results for every ROI. Overall, in regions with a significant difference relative to individuals without mutations, rates of Aβ deposition were significantly higher in those with mutations at a mean of 18·9 years (SD 3·3) before expected symptom onset, metabolism began to differ between carriers and non-carriers at a mean of 14·1 years (SD 5·1) before expected symptom onset, and MRI structural measures differed between carriers and controls (declined) at a mean of 4·7 years (SD 4·2) before expected symptom onset.

Figure 2 depicts the first point in the disease relative to the estimated expected age at symptom onset at which rates of biomarker change in that cortical region are significantly different between mutation carriers and non-carriers. The differences across regions and methods reflect the temporal and spatial evolution of pathology

	Non-carriers (n=148)	Asymptomatic carriers (n=141)	Symptomatic carriers (n=88)
Women	85 (57%)	78 (55%)	49 (56%)
Men	63 (43%)	63 (45%)	39 (44%)
Age (years)	39·5 (11·4)	34·6 (9·2)	45·7 (9·9)
MMSE	29·0 (2·7)	28·8 (2·7)	23·9 (10·2)
CDR-SOB	0·0 (0·2)	0·0 (0·1)	3·6 (3·5)
EYO (years)	–8·9 (11·4)	–13·7 (9·2)	0·5 (7·1)
PSEN1	122 (82%)	117 (83%)	76 (86%)
PSEN2	17 (11%)	16 (11%)	6 (7%)
APP	9 (6%)	8 (6%)	6 (7%)
Number with follow-up	70 (47%)	73 (52%)	58 (66%)
Number of visits*	2·3 (0·8)	2·3 (0·8)	2·8 (1·2)
Follow-up (years)*	3·0 (1·7)	3·0 (1·6)	2·0 (1·3)

Data are n (%) or mean (SD). *Summary values are only for those individuals with longitudinal data. EYO=estimated years to onset. MMSE=Mini-Mental State Examination. CDR-SOB=clinical dementia rating scale sum of boxes. *PSEN1*=presenilin 1. *PSEN2*=presenilin 2. *APP*=amyloid precursor protein.

Table 1: **Study demographics at baseline and duration of follow-up**

	^{11}C-PIB PET	^{18}F-FDG PET	MRI
One visit	184	177	176
Two visits	124	131	145
Three visits	23	27	35
Four visits	10	11	11
Five visits	4	5	8
Six visits	1	1	2
Total participants	346	352	377

^{11}C-PIB=^{11}C-Pittsburgh Compound B. FDG=^{18}F-Fluorodeoxyglucose.

Table 2: **Summary of imaging data**

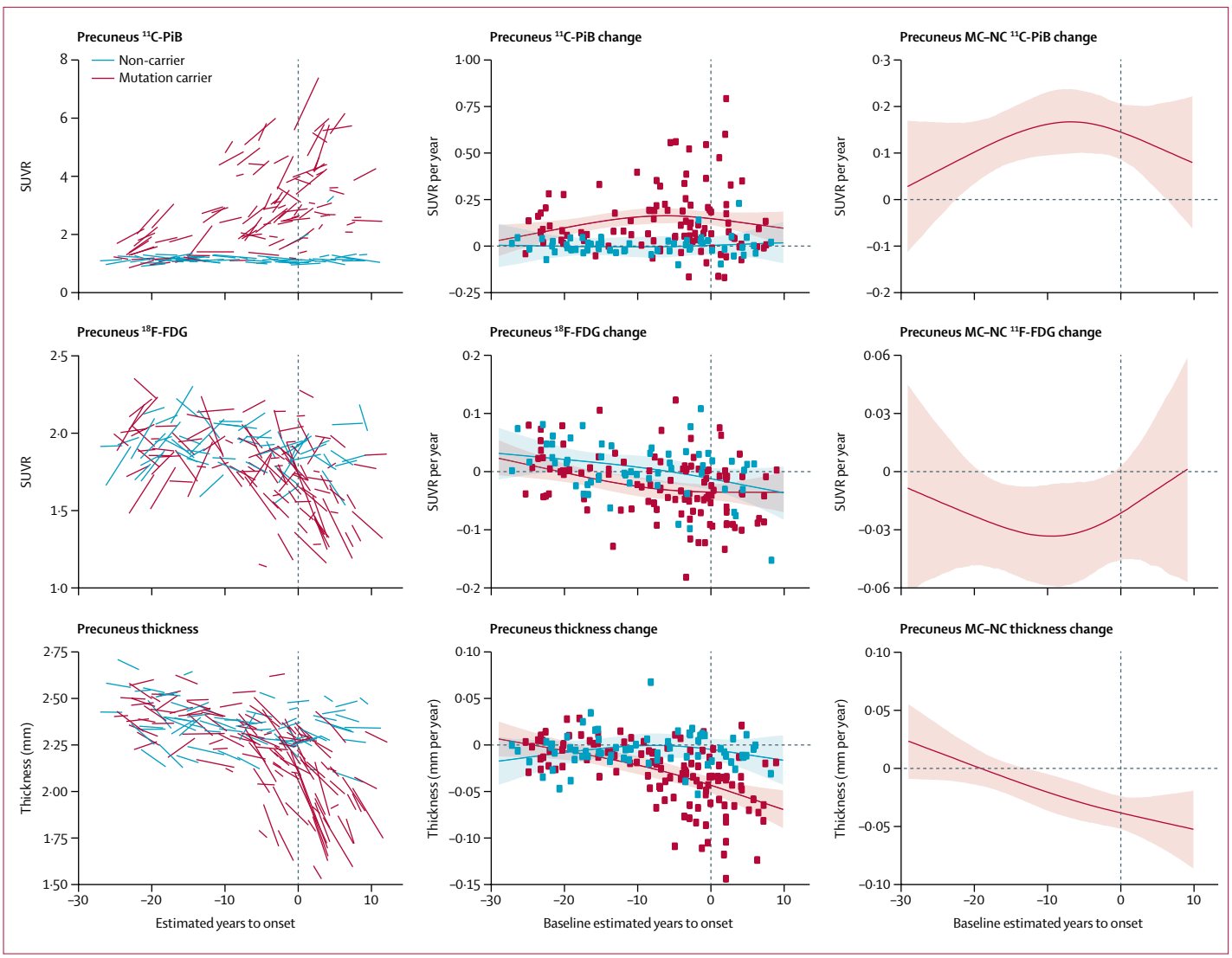

Figure 1: **Modelling longitudinal change in the precuneus**
The left-hand panels depict the model estimates of longitudinal biomarkers. The middle panels depict the estimated rate of change across the course of the disease for mutation carriers and non-carriers. Individual random-effect slope estimates are plotted as coloured dots. The right-hand panels depict the difference in rate of biomarker change between mutation carriers and non-carriers across the course of the disease. For both the middle and right-hand panels the shaded areas represent 99% credible intervals around the model estimates. The credible intervals are drawn from the actual distributions of model fits derived by the Hamilton Markov chain Monte Carlo analyses. Any point in these difference curves where the shaded area is not touching the zero axis is a point in the disease progression (as measured by estimated years to onset) where the biomarker accumulation rate is different between groups. The first estimated years to onset point that was significantly different between groups was considered the initial divergence between groups. Figures depicting the model results for every region of interest are available via a link in the appendix. To avoid inadvertently revealing mutation status, figures are displayed with baseline estimated years to onset –29 to +10. ^{11}C-PIB=^{11}C-Pittsburgh Compound B. ^{18}F-FDG=^{18}F-Fluorodeoxyglucose. SUVR=standardised uptake value ratios. MC–NC=mutation carrier–non-carrier.

over the course of the disease. Rates of biomarker change in regions that are grey were not significantly different between groups. This information is presented in numerical form in the appendix. Many regions follow trajectories similar to the precuneus; however, the emergence of pathology varied throughout the brain. Furthermore, there were regional differences by method; for example, relative to non-carriers the superior temporal lobe did not show a metabolic loss in mutation carriers, but had atrophy changes at 5·6 years before expected symptom onset. Figure 3 depicts rates of change in mutation carriers for three cortical and three subcortical regions that exemplify common patterns.

For ^{11}C-PiB PET, 32 of 34 cortical regions showed significantly greater longitudinal rates of accumulation in mutation carriers relative to non-carriers. The first point of divergence between groups varied across regions (22·2 years before expected symptom onset to 2·5 years before), with the precuneus, posterior cingulate gyrus, and medial orbital frontal cortex regions showing the earliest changes (around 21 years before expected symptom onset). Of the 32 regions with significant

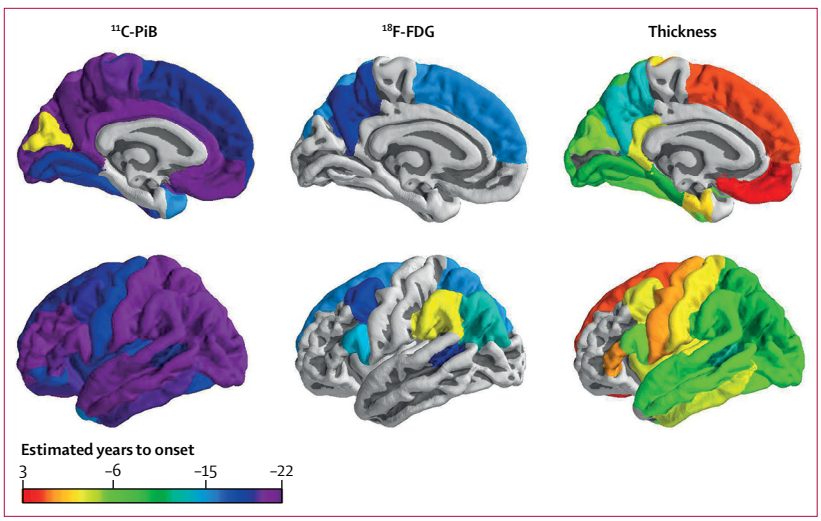

Figure 2: **Emergence of differences in neuroimaging biomarkers**
The colour scale represents the first point in the disease relative to estimated years to onset at which rates of biomarker change in that cortical region are significantly different between mutation carriers and non-carriers (akin to the first point where credible interval are different from zero in figure 1 right panels). There is a temporal evolution where increased Aβ deposition precedes hypometabolism that in turn is followed by cortical thinning. Information for all methods and regions is presented in numerical form in the appendix. ^{11}C-PIB=^{11}C-Pittsburgh Compound B. ^{18}F-FDG=^{18}F-Fluorodeoxyglucose.

See Online for videos

differences, these differences occurred more than 15 years before expected symptom onset in all but the cuneus (2·5 years). Of the seven subcortical regions, the accumbens (22·2 years before expected symptom onset), putamen (17·0 years before), and caudate (16·4 years before) showed greater ^{11}C-PiB accumulation rates in mutation carriers whereas the amygdala, hippocampus, palladium, and thalamus did not differ. Significant differences in progressive hypometabolism in mutation carriers relative to non-carriers were less pronounced, with eight of 34 cortical regions showing significant interactions. The effects were apparent 18·8–2·8 years before the expected symptom onset, with the earliest effects detected in the precuneus, banks of the superior temporal sulcus, and caudal middle frontal cortex (around 18 years before). No subcortical regions showed significant differences in the rate of ^{18}F-FDG change. For MRI, 24 of 34 cortical areas and four of seven subcortical areas showed increased rates of atrophy in mutation carriers relative to non-carriers with effects appearing from 13 years before to 2·3 years after expected symptom onset. The precuneus (13·0 years before expected symptom onset), banks of the superior temporal sulcus (11·5 years before), and inferior parietal cortex (10·6 years before) showed the earliest changes.

We also observed regional differences in the rates of biomarker change within the mutation carrier group. A direct comparison of the rates of biomarker change between regions is presented in the appendix. In the precuneus there was a rapid increase in Aβ deposition; this rate peaked but remained positive even after the predicted onset of dementia (figure 3 and figure 4). This was the most common pattern across areas. In other regions (eg, the insula) initial accelerations in Aβ deposition were followed by decelerations, leading to a plateau of total Aβ levels. In a subset of regions (eg, the inferior temporal cortex) the estimated rate of Aβ accumulation accelerates throughout the disease. Once declining, glucose metabolism in the precuneus showed prominent and worsening rates of hypometabolism before the rates stabilised at 5 years before the expected symptom onset; in the inferior temporal cortex, the rate of metabolic loss modestly increased initially before quickly plateauing (figure 3). Many regions had relatively small rates of metabolic decline in mutation carriers, even approaching the expected age of symptom onset. In regions with structural decline the trajectories were fairly consistent, with the rate of atrophy accelerating as the disease progressed. However, the absolute rate of decline was often different between regions. Matrices directly comparing the regional rates of change for each biomarker at different timepoints (25, 15, and 5 years before, and 5 years after the expected age of onset) can be found in the appendix. We created voxel-wise movies that depict the rate of change and total biomarker levels in mutation carriers (video 1, video 2, video 3) and the creation of these movies is detailed in the appendix.

Discussion

Alzheimer's disease is not static but possesses dynamism, in terms of which pathological processes appear first and how such pathology propagates throughout the brain. Because dementia onset is predictable in autosomal dominant Alzheimer's disease, it provides an elegant model with which to examine pathological staging. Characterisation of the spatial and temporal spread of pathology provides insight into the pathophysiology of the disease, informs how neuroimaging could aid recruitment of participants in clinical trials, and is crucial if we are to be able to assess the efficacy of interventions on longitudinal biomarker measurements.

The primary goal of the current analysis was to find the first biomarker timepoint in the course of the disease at which carriers of autosomal dominant Alzheimer's disease mutations showed different rates of pathological progression relative to non-carrier family members. This timepoint can be interpreted as the moment at which longitudinal change in that brain area due to Alzheimer's disease can first be detected with in-vivo neuroimaging. The primary analyses using this approach focused on regional differences across the brain within a marker (eg, precuneus *vs* parietal ^{11}C-PiB PET) as well as comparing spatial differences between biomarkers (eg, ^{11}C-PiB PET *vs* ^{18}F-FDG PET).

Consistent with previous work[7] we found that Aβ deposition was the first biomarker to show differences between mutation groups. Mutation carriers had greater Aβ deposition than did non-carriers more than 20 years

before the expected age of symptom onset. Aβ increases were near ubiquitous, with most regions accumulating pathology more than 14 years before the expected year of dementia onset. Measures of metabolism in autosomal dominant Alzheimer's disease represent overlapping maturational and disease changes. Both non-carriers and

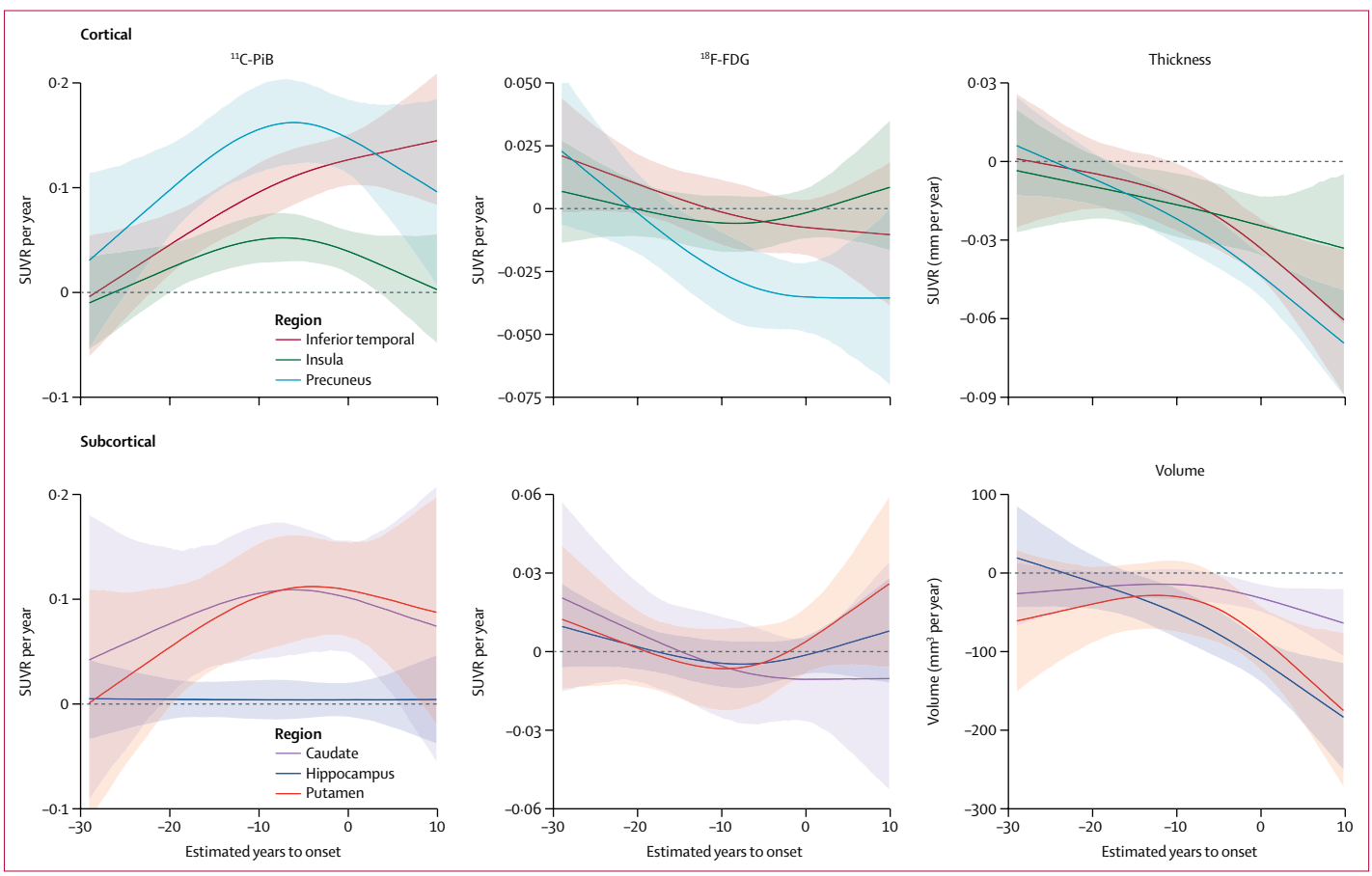

Figure 3: **Trajectories of biomarker accumulation in mutation carriers**
Data are for three cortical and three subcortical regions for ^{11}C-PiB, ^{18}F-FDG, and structural MRI that highlight different patterns of change seen in different brain regions. ^{11}C-PIB=^{11}C-Pittsburgh Compound B. ^{18}F-FDG=^{18}F-Fluorodeoxyglucose. SUVR=standardised uptake value ratios.

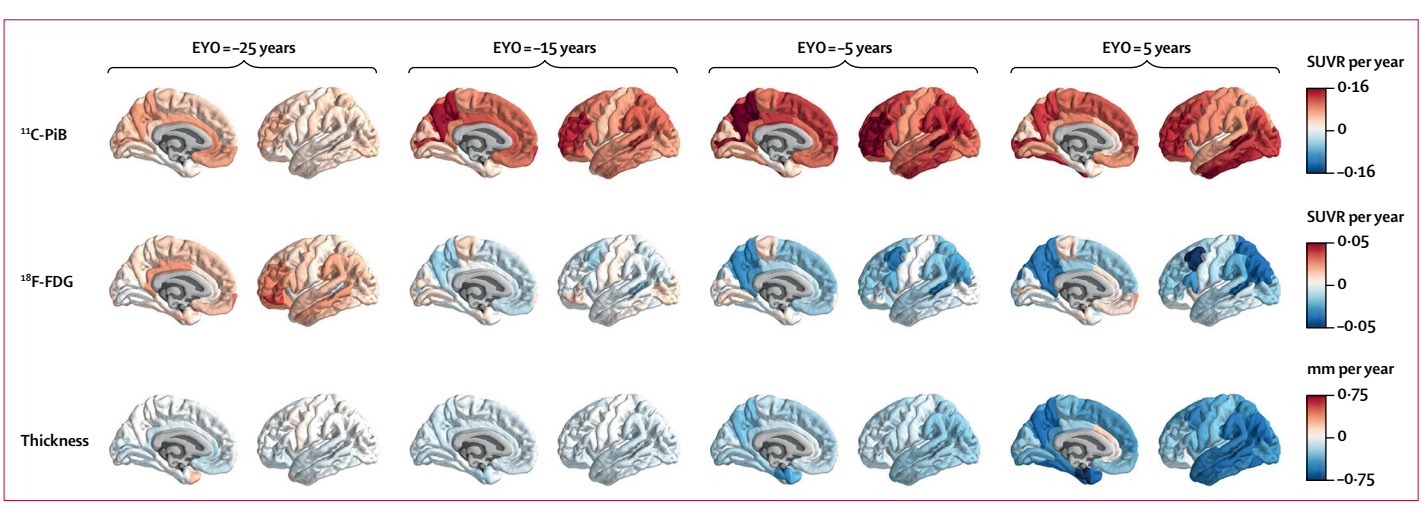

Figure 4: **Depictions of model estimates of rate of change in ^{11}C-PiB, ^{18}F-FDG, and cortical thickness**
Data are from mutation carriers. ^{11}C-PIB=^{11}C-Pittsburgh Compound B. ^{18}F-FDG=^{18}F-Fluorodeoxyglucose. SUVR=standardised uptake value ratios. EYO=estimated years to onset.

mutation-carrying cohorts had inverted U-shaped trajectories, with the absolute levels of glucose metabolism initially modestly increasing with estimated years from expected symptom onset, followed by a prolonged decrease. The key difference is that mutation carriers showed metabolic reductions earlier and to a greater degree than did non-carriers. Although cross-sectional values still overlapped between groups early in the disease, longitudinal trajectories reveal divergence (appendix). The precuneus showed the earliest metabolic decrease at 18·8 years before the estimated expected age of onset, with significant regions on average becoming hypometabolic at a mean of 14·1 years before the estimated expected age of onset. Reductions in grey matter thickness and volume were the last neuroimaging biomarker to manifest differences between mutation carries and non-carriers, which occurred over the majority of the brain. Again, the precuneus was the earliest region to differ between carriers and non-carriers, with declines emerging a decade before estimated dementia onset, while overall declines were most prolific in the 5 years preceding expected dementia onset.

The relationships between the three biomarkers are complex. Although all regions with metabolic decreases have abnormal Aβ accumulation, many regions with abnormal Aβ accumulation rates did not show elevated metabolic decline. Although ^{18}F-FDG hypometabolism and structural decline are markers of degeneration, our results indicate they can be incongruent. In regions in which they both occur, declines in glucose metabolism precede atrophy by about 5–10 years. However, there are regions that showed β-amyloidosis and structural atrophy where significant metabolic decline was not detected (eg, the occipital and temporal regions). Portions of the medial temporal lobe (eg, the hippocampus) did not manifest pathological change in ^{11}C-PiB PET or ^{18}F-FDG PET, but had structural declines. Although there is generally a tripartite hierarchy such that β-amyloidosis precedes metabolic decline that in turn precedes atrophy, these relationships are highly heterogeneous across the cortex.

Discordance between imaging biomarkers has been noted in sporadic Alzheimer's disease.[37–44] Owing to the cross-sectional nature of most of the work, such spatial incongruences could be due to temporal lags in the emergence of pathologies.[42,44] Estimated year of expected symptom onset, as a marker of disease time, is perfectly suited to detect such temporal evolutions. The current work does indeed clearly show that a temporal progression is present in some regions (eg, changes are first detected by ^{11}C-PiB, then ^{18}F-FDG PET, and then cortical thinning in the precuneus). However, despite the long disease window covered by the current study population, some regions still show only a subset of pathologies. This suggests the incongruences are not simply a product of temporal lag, but can represent true heterogeneity. Other, unobserved, biomarkers such as those that measure tau pathology and inflammation, might help explain this heterogeneous relationship.

To our knowledge, the current work presents the largest and most comprehensive analysis of neuroimaging data in autosomal dominant Alzheimer's disease to date. Still, the majority of longitudinal participants had only a limited follow-up (mean 2·4 visits); results at the edges of the estimated year of expected symptom onset range, at which outliers have disproportional influence, must be interpreted with care. Only small numbers of participants had *PSEN2* or *APP* mutations. As the DIAN study gains more timepoints, longitudinal estimates will be improved further and it might be possible to compare the three types of mutation. A greater number of individuals and timepoints will also increase the feasibility of modelling multiple methods simultaneously across all brain regions as previously done using aggregate measures of pathology.[45]

The temporal and spatial ordering of biomarkers must also be interpreted with caveats. No one individual has data across the entire disease window, and our results represent population rather than individual participant effects. Furthermore, as seen in regional fits of the data, some individuals differ from population trajectories. Thus, imaging data alone might not be sufficient to make individual-level disease stage predictions. Such predictions would require further work that accounts for individual differences due to factors such as genetic variability and lifestyle. The current work also uses partial volume corrected PET data;[27,28] analyses without this step could have slightly different trajectories late in the disease.

The temporal ordering of biomarker change should also be viewed as relative rather than absolute. Our models are fit using a particular definition of estimated year of expected symptom onset. Supplemental models using a modified definition indicate a preserved relative ordering (eg, precuneus Aβ then hypometabolism then structural decline) but slight differences in absolute timing (eg, shifts from 22·2 years to 19·8 years before expected symptom onset; appendix). Furthermore, our results reflect the first detectable changes with PET and MRI, which are constrained by the inherent sensitivities and signal-to-noise properties of the imaging techniques. The current analyses use the cerebellum as a reference region for PET. Results using the brainstem instead were essentially unchanged (appendix). Finally, although autosomal dominant Alzheimer's disease can serve as a model for sporadic Alzheimer's disease, direct comparisons should explore potential differences.

Our results reveal complex patterns of biomarker accumulation across the brain. Elevations in β-amyloidosis occur more than two decades before, and continue to accrue even after, the expected year of symptom onset. Neurodegeneration measured with both ^{18}F-FDG and structural MRI begins while Aβ is still increasing and occurs closer in time to, but still well before, the onset of

dementia. While global measures are likely to capture a large degree of intraindividual variability, our results indicate not just when, but where pathology emerges in the brain. Understanding such longitudinal change provides insight into the pathophysiological progression of Alzheimer's disease and has implications for the selection of participants and endpoints for clinical trials.

Contributors

BAG and TMB contributed equally to the present work and wrote the manuscript, analysed the data, and generated the figures and movies. YS, AH, AD, SF, JC, CRJ, and MMW oversaw data quality control and processing. CX, NJC, JH, DSM, AMF, DMH, RCH, KLP, EM, GW, MER, JCM, RJB, and TLSB and oversaw overall study design and general implementation. RJB and TLSB assisted in data interpretation. BMA, SBB, AMB, DMC, JPC, SC, StF, NCF, NRG, CF, JL, CLM, MNR, SS, AJS, PRS, and PMT oversaw study implementation and data collection at their respective institutions. All authors revised the manuscript.

Declaration of interests

BAG and BMA report participating in a clinical trial of AV-1451 sponsored by Avid Radiopharmaceuticals. EM reports grants from Dominantly Inherited Alzheimer Network Trials Unit Pharma Consortium, outside the submitted work. CX reports grants from the National Institute on Aging (NIA) outside the submitted work. JH reports personal fees from Biogen and Lundbeck, outside the submitted work. CRJ reports consulting services for Lilly Co and grants from National Institutes of Health (NIH), outside the submitted work. DSM reports grants from NIH and support from Radiologics, both outside the conduct of the study. AMF reports personal fees from DiamiR, LabCorp, IBL International, and Genentech and grants from Roche Diagnostics, Fujirebio, and Biogen, outside the submitted work. DMC reports grants from the Alzheimer's Society, during the conduct of the study. JL reports grants from German Ministry of Research and Education, during the conduct of the study. AJS reports non-financial support from Avid Radiopharmaceuticals and grants from Eli Lilly, outside the submitted work. SBB reports grants from NIH, during the conduct of the study; clinical trial participation from Lundbeck, and clinical trial participation from Grifols Biologicals, outside the submitted work. MNR reports support from Servier and Merck outside the submitted work. NCF reports personal fees from Janssen, Roche/Genentech, Janssen Alzheimer's Immunotherapy, Eli Lilly, Novartis Pharma AG, Sanofi GSK, and Biogen, outside the submitted work. NRG reports receipt of an Eli Lilly Multi center Treatment Study Grant, receipt of a Biogen Multi center Treatment Study Grant, and Cytox consultation. PRS reports grants from NIH and NIA, the Anonymous Foundation, the Mason Foundation, and the Roth Charitable Foundation during the conduct of the study; personal fees from ICMI Speakers and Entertainers, outside the submitted work; and serving as the Interim Director of the Australian National Health and Medical Research Council (NHMRC). DMH cofounded and is on the scientific advisory board of C2N Diagnostics. DMH is an inventor on a submitted patent "Antibodies to Tau" that is licensed by Washington University to C2N Diagnostics. This patent was subsequently licensed to AbbVie. DMH is an inventor on patents licensed by Washington University to Eli Lilly and Company based on intellectual property related to the anti-Abeta antibody solanezumab. DMH consults for Genentech, AbbVie, Eli Lilly, GlaxoSmithKline, Proclara Biosciences, and Denali. MMW reports grants from NIH, NIA, and National Institute of Mental Health, Department of Defense, CA Department of Public Health, Larry L Hillblom Foundation, the Patient-Centered Outcomes Research Institute, Global Alzheimer's Platform Foundation, and Monell Chemical Senses Center; grants from and consulting for Alzheimer's Drug Discovery Foundation (ADDF) and the Alzheimer's Association; scientific advisory board participation and consulting for Pfizer, scientific advisory board participation, consulting for, and stock options from Alzheon, scientific advisory board participation and consulting for Eli Lilly, scientific advisory board participation for Dolby Ventures, scientific advisory board participation for ADNI, editorial board participation for MRI Magazine, editorial board participation for Alzheimer's & Dementia Magazine, consulting for Synarc, consulting for Janssen, consulting for Accera Pharma, consulting for Avid Radiopharma, consulting for Araclon, consulting and scientific advisory board participation for Merck, consulting for Scienomics Group, consulting for AVOS Consulting, consulting for INC Research, consulting for Biogen Idec, consulting for BioClinica, consulting for Howard University, consulting for Guidepoint, consulting for GLG Research, consulting for Genentech, and stock options from Alzeca, outside the submitted work. PMT reports grants from NIA, NIBIB, and National Institute of Biomedical Imaging and Bioengineering and National Institute on Neurological Disorders and Stroke outside the submitted work. JCM reports grants from NIH (P50AG005681, P01AG003991, P01AG026276, and UF01AG032438), during the conduct of the study; consultancy fees from Lilly USA, outside the submitted work. RJB reports grants from NIH/NIA (U19AG32438) and an anonymous foundation, during the conduct of the study, grants from Eli Lilly, Roche, Pharma Consortium (Abbvie, AstraZeneca, Biogen, Eisai, Eli Lilly and Co, Hoffman La-Roche, Janssen, Pfizer, Sanofi-Aventis), and Tau SILK/PET Consortium (Biogen, Abbvie, and Lilly), non-financial support from Avid Radiopharmaceuticals, personal fees and intellectual property rights (patent co-inventor) from Washington University, personal fees and non-financial support from Roche, IMI, FORUM, and Pfizer, and personal fees from Merck, Johnson and Johnson, outside the submitted work. TLSB reports grants, non-financial support and clinical trial pariticipation from Avid Radiopharmaceuticals/Eli Lilly, and clinical trial participation from Roche, outside the submitted work. TMB, YS, AH, AD, SF, JC, GW, NJC, RCH, KLP, AMB, JPC, SC, StF, CF, CLM, SS, and MER declare no competing interests.

Acknowledgments

Foremost, we wish to acknowledge the dedication of the participants and their families, without whom these studies would not be possible. We additionally thank all of the participating researchers in the Dominantly Inherited Alzheimer Network. This research was funded by the National Institutes of Health (NIH; UFAG032438, UL1TR000448, P30NS098577, R01EB009352), the German Center for Neurodegenerative Diseases (DZNE), the National Institute for Health Research (NIHR) Queen Square Dementia Biomedical Research Centre, and the Medical Research Council Dementias Platform UK (MR/L023784/1 and MR/009076/1). We acknowledge the financial support of Fred Simmons and Olga Mohan, the Barnes-Jewish Hospital Foundation, the Charles F and Joanne Knight Alzheimer's Research Initiative, the Hope Center for Neurological Disorders, the Mallinckrodt Institute of Radiology, and the Paula and Rodger Riney fund. Computations were performed using the facilities of the Washington University Center for High Performance Computing, which were partially funded by NIH grants (1S10RR022984–01A1 and 1S10OD018091–01).

References

1 Pike KE, Savage G, Villemagne VL, et al. β-amyloid imaging and memory in non-demented individuals: evidence for preclinical Alzheimer's disease. *Brain* 2007; **130:** 2837–44.

2 Hardy JA, Higgins GA. Alzheimer's disease: the amyloid cascade hypothesis. *Science* 1992; **256:** 184–85.

3 Jack CR, Knopman DS, Jagust WJ, et al. Tracking pathophysiological processes in Alzheimer's disease: an updated hypothetical model of dynamic biomarkers. *Lancet Neurol* 2013; **12:** 207–16.

4 Moulder KL, Snider BJ, Mills SL, et al. Dominantly Inherited Alzheimer Network: facilitating research and clinical trials. *Alzheimers Res Ther* 2013; **5:** 48.

5 Ryman DC, Acosta-Baena N, Aisen PS, et al. Symptom onset in autosomal dominant Alzheimer disease: a systematic review and meta-analysis. *Neurology* 2014; **83:** 253–60.

6 Bateman RJ, Xiong C, Benzinger TLS, et al. Clinical and biomarker changes in dominantly inherited Alzheimer's disease. *N Engl J Med* 2012; **367:** 795–804.

7 Benzinger TLS, Blazey T, Jack CR, et al. Regional variability of imaging biomarkers in autosomal dominant Alzheimer's disease. *Proc Natl Acad Sci USA* 2013; **110:** E4502–09.

8 Fleisher AS, Chen K, Quiroz YT, et al. Associations between biomarkers and age in the presenilin 1 E280A autosomal dominant Alzheimer disease kindred: a cross-sectional study. *JAMA Neurol* 2015; **72:** 316–24.

9 Yau W-YW, Tudorascu DL, McDade EM, et al. Longitudinal assessment of neuroimaging and clinical markers in autosomal dominant Alzheimer's disease: a prospective cohort study. *Lancet Neurol* 2015; **14**: 804–13.

10 Weston PSJ, Nicholas JM, Lehmann M, et al. Presymptomatic cortical thinning in familial Alzheimer disease: A longitudinal MRI study. *Neurology* 2016; **87:** 2050–57.

11 Wang F, Gordon BA, Ryman DC, et al. Cerebral amyloidosis associated with cognitive decline in autosomal dominant Alzheimer disease. *Neurology* 2015; **87:** 2050–57.

12 Sala-Llonch R, Lladó A, Fortea J, et al. Evolving brain structural changes in PSEN1 mutation carriers. *Neurobiol Aging* 2015; **36:** 1261–70.

13 Schott JM, Fox NC, Frost C, et al. Assessing the onset of structural change in familial Alzheimer's disease. *Ann Neurol* 2003; **53:** 181–88.

14 Fagan AM, Xiong C, Jasielec MS, et al. Longitudinal change in CSF biomarkers in autosomal-dominant Alzheimer's disease. *Sci Transl Med* 2014; **6:** 226ra30.

15 Knight WD, Kim LG, Douiri A, Frost C, Rossor MN, Fox NC. Acceleration of cortical thinning in familial Alzheimer's disease. *Neurobiol Aging* 2011; **32:** 1765–73.

16 Kinnunen KM, Cash DM, Poole T, et al. Presymptomatic atrophy in autosomal dominant Alzheimer's disease: a serial MRI study. *Alzheimers Dement* 2018; **14:** 45–53.

17 Thompson WK, Hallmayer J, O'Hara R, Alzheimer's Disease Neuroimaging Initiative. Design considerations for characterizing psychiatric trajectories across the lifespan: application to effects of APOE-ε4 on cerebral cortical thickness in Alzheimer's disease. *Am J Psychiatry* 2011; **168:** 894–903.

18 Xu Z, Shen X, Pan W, et al. Longitudinal analysis is more powerful than cross-sectional analysis in detecting genetic association with neuroimaging phenotypes. *PLoS One* 2014; **9:** e102312.

19 Mills SM, Mallmann J, Santacruz AM, et al. Preclinical trials in autosomal dominant AD: implementation of the DIAN-TU trial. *Rev Neurol* 2013; **169**: 737–43.

20 Reiman EM, Langbaum JBS, Fleisher AS, et al. Alzheimer's prevention initiative: a plan to accelerate the evaluation of presymptomatic treatments. *J Alzheimers Dis* 2011; **26** (suppl 3)**:** 321–29.

21 Sperling RA, Rentz DMM, Johnson KA, et al. The A4 study: stopping AD before symptoms begin? *Sci Transl Med* 2014; **6:** 228fs13.

22 Morris JC. The Clinical Dementia Rating (CDR): current version and scoring rules. *Neurology* 1993; **43:** 2412–14.

23 Jack CCR, Bernstein MA, Borowski BBJ, et al. Update on the magnetic resonance imaging core of the Alzheimer's disease neuroimaging initiative. *Alzheimers Dement* 2010; **6:** 212–20.

24 Fischl B. FreeSurfer. *Neuroimage* 2012; **62:** 774–81.

25 Fischl B, Dale AMM. Measuring the thickness of the human cerebral cortex from magnetic resonance images. *Proc Natl Acad Sci USA* 2000; **97:** 11050–55.

26 Su Y, D'Angelo GM, Vlassenko AG, et al. Quantitative Analysis of PiB-PET with FreeSurfer ROIs. *PLoS One* 2013; **8:** e73377.

27 Su Y, Blazey TM, Snyder AZ, et al. Partial volume correction in quantitative amyloid imaging. *Neuroimage* 2015; **107:** 55–64.

28 Rousset OG, Ma Y, Evans AC. Correction for partial volume effects in PET: principle and validation. *J Nucl Med* 1998; **39:** 904–11.

29 Joshi A, Koeppe RA, Fessler JA. Reducing between scanner differences in multi-center PET studies. *Neuroimage* 2009; **46:** 154–59.

30 Bernal-Rusiel JL, Reuter M, Greve DN, Fischl B, Sabuncu MR. Spatiotemporal linear mixed effects modeling for the mass-univariate analysis of longitudinal neuroimage data. *Neuroimage* 2013; **81**: 358–70.

31 Bernal-Rusiel JL, Greve DN, Reuter M, Fischl B, Sabuncu MR. Statistical analysis of longitudinal neuroimage data with Linear Mixed Effects models. *Neuroimage* 2013; **66:** 249–60.

32 Bilgel M, Prince JL, Wong DF, Resnick SM, Jedynak BM. A multivariate nonlinear mixed effects model for longitudinal image analysis: Application to amyloid imaging. *Neuroimage* 2016; **134:** 658–70.

33 Jack CR, Wiste HJ, Lesnick TG, et al. Brain β-amyloid load approaches a plateau. *Neurology* 2013; **80:** 890–96.

34 Jack CR, Vemuri P, Wiste HJ, et al. Shapes of the trajectories of 5 major biomarkers of Alzheimer disease. *Arch Neurol* 2012; **69:** 856–67.

35 Carpenter B, Lee D, Brubaker MA, et al. Stan: a probabilistic programming language. *J Stat Softw* 2017; published online Jan 11. DOI:10.18637/jss.v076.i01.

36 Gelman A, Lee D, Guo J. Stan: a probabilistic programming language for bayesian inference and optimization. *J Educ Behav Stat* 2015; **40:** 530–43.

37 Gordon BA, Blazey T, Benzinger TL. Regional variability in Alzheimer's disease biomarkers. *Future Neurol* 2014; **9:** 131–34.

38 La Joie R, Perrotin A, Barré L, et al. Region-specific hierarchy between atrophy, hypometabolism, and β-amyloid (Aβ) load in Alzheimer's disease dementia. *J Neurosci* 2012; **32:** 16265–73.

39 Grothe MJ, Teipel SJ. Spatial patterns of atrophy, hypometabolism, and amyloid deposition in Alzheimer's disease correspond to dissociable functional brain networks. *Hum Brain Mapp* 2016; **37:** 35–53.

40 Edison P, Archer HA, Hinz R, et al. Amyloid, hypometabolism, and cognition in Alzheimer disease: an [11C]PIB and [18F]FDG PET study. *Neurology* 2007; **68:** 501–08.

41 Lehmann M, Ghosh PM, Madison C, et al. Diverging patterns of amyloid deposition and hypometabolism in clinical variants of probable Alzheimer's disease. *Brain* 2013; **136:** 844–58.

42 Förster S, Grimmer T, Miederer I, et al. Regional expansion of hypometabolism in Alzheimer's disease follows amyloid deposition with temporal delay. *Biol Psychiatry* 2012; **71:** 792–97.

43 Alexopoulos P, Kriett L, Haller B, et al. Limited agreement between biomarkers of neuronal injury at different stages of Alzheimer's disease. *Alzheimers Dement* 2014; **10:** 684–89.

44 Förster S, Yousefi BH, Wester H-J, et al. Quantitative longitudinal interrelationships between brain metabolism and amyloid deposition during a 2-year follow-up in patients with early Alzheimer's disease. *Eur J Nucl Med Mol Imaging* 2012; **39:** 1927–36.

45 Donohue MC, Jacqmin-Gadda H, Le Goff M, et al. Estimating long-term multivariate progression from short-term data. *Alzheimers Dement* 2014; **10:** S400–10.